The Constitución earthquake of 25 March 2012: A large aftershock of the Maule earthquake near the bottom of the seismogenic zone

Sergio Ruiz [a,*], Raphael Grandin [b], Viviana Dionicio [b], Claudio Satriano [b], Amaya Fuenzalida [c], Christophe Vigny [c], Eszter Kiraly [b], Clio Meyer [c], Juan Carlos Baez [d], Sebastian Riquelme [a], Raúl Madariaga [c], Jaime Campos [a]

[a] *Departamento de Geofísica, Facultad de Ciencias Físicas y Matemáticas, Universidad de Chile, Santiago, Chile*
[b] *Institut de Physique du Globe de Paris, Sorbonne Paris Cité, Univ Paris Diderot, UMR 7154 CNRS, F-75005 Paris, France*
[c] *Laboratoire de Géologie, École Normale Supérieure, Paris, France*
[d] *Departamento de Ciencias Geodésicas, Campus Los Angeles, Universidad de Concepcion, Los Angeles, Chile*

ARTICLE INFO

ABSTRACT

The Mw 7.0 Constitución earthquake of March 2012 is one of the largest interplate aftershocks of the Maule 2010 Mw 8.8 mega-thrust earthquake. This event was recorded by high-rate GPS stations, local seismometers and accelerometers, the Global Seismographic Network and SAR acquisitions by the ENVISAT satellite. We have used these data to perform a kinematic inversion and back projection to identify the principal characteristics of this event. The Constitución earthquake nucleated at 39 km depth and then propagated up-dip at subshear speed towards its centroid, with an unusually long initiation phase that lasted almost 6 s. The largest slip of this event was located in the deeper part of the subduction interface, between the region of maximum co-seismic slip of the 2010 Maule earthquake, and the area where rapid afterslip occurred following that event. Features of the Constitución earthquake may suggest that larger interplate aftershocks of the Maule event preferentially occur in the deeper part of the plate interface where ruptures are complex, produce high frequencies and involve numerous asperities.

© 2013 Elsevier B.V. All rights reserved.

1. Introduction

On 25 March 2012, a large Mw 7.0 interplate aftershock of the 27 February 2010 (06:34 UT) Mw 8.8 Maule mega-thrust earthquake occurred near Constitución, close to the area of maximum damage caused by the Maule event (Astroza et al., 2012). At the present time, this is one of the largest interplate thrust aftershocks of the Maule earthquake. The main aftershocks have been the Mw 7.4 27 February 2010 (08:01 UT) event that occurred in the outer rise of the Nazca plate west of the trench; the Mw 6.9–7.0 11 March 2010 Pichilemu earthquakes (Farías et al., 2011; Ryder et al., 2012) which occurred on shallow normal crustal faults, and the Mw 7.2 thrust aftershock of 2 January 2011, located in the southern part of the Maule 2010 rupture. The epicenter of the Constitución earthquake is located where the rupture zones of the 2010 Maule mega-thrust earthquake and that of the Mw 7.7 Talca earthquake of 1 December 1928 overlap.

The 27 February 2010 Mw 8.8 Maule mega-thrust earthquake was characterized by a large rupture zone of roughly 500 km ×

200 km (Vigny et al., 2011; Moreno et al., 2012; Ruiz et al., 2012; and references therein). The rupture propagated bilaterally to the north and to the south from a nucleation site located close to 36°S. While the southern half of the rupture area corresponds to the entire "Constitución–Concepcion seismic gap" identified as the site of a previous earthquake of M ∼ 8.5 in 1835 (Campos et al., 2002; Ruegg et al., 2009), a significant part of the seismic moment during the Maule earthquake was released in the northern half of the rupture area where large events had occurred in the last century: the M = 7.7 Talca 1928 earthquake, the M = 8.5 1906 and the M = 8.0 1985 Valparaíso earthquakes. Unfortunately, limited information on the exact location of slip during the pre-instrumental period makes it difficult to assess the amount of overlap between these earthquakes. Only the 1985 earthquake was studied using teleseismic and some strong motion records (Mendoza et al., 1994; Ruiz et al., 2011), its rupture extends southward to ∼35.5°S.

The northern end of the rupture zone of the Maule event (34.0°S–34.5°S) contains the bulk of the 2010–2011 aftershock activity (Lange et al., 2012; Rietbrock et al., 2012). The 2012 Constitución earthquake occurred at the latitude of largest slip release of the 2010 Maule earthquake, around ∼35°S (see Fig. 1) and it overlaps with the rupture zone of the Mw 7.7 Talca earthquake of
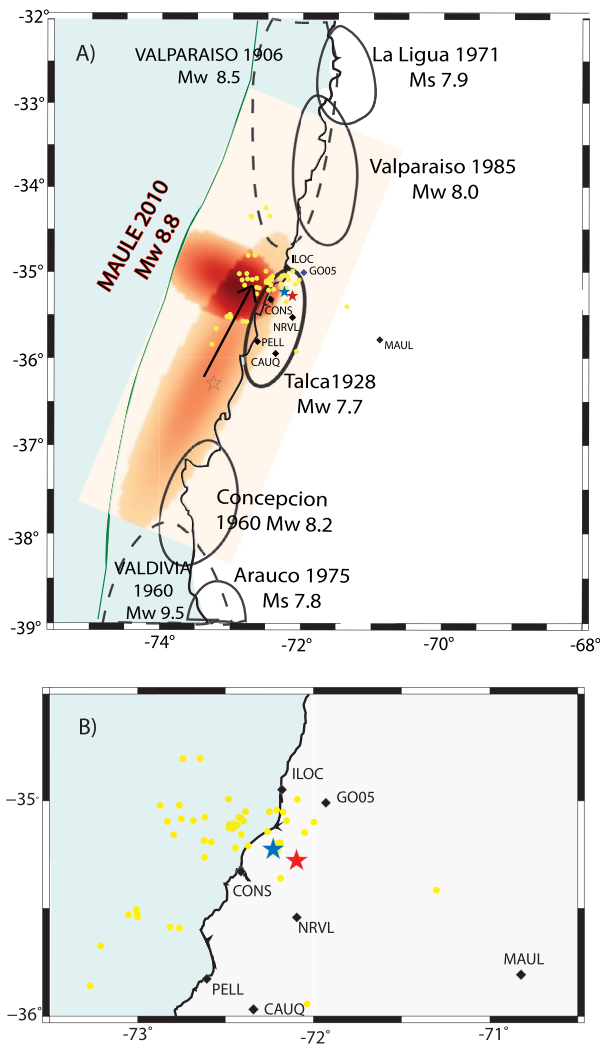
Fig. 1. The Mw 7.0 Constitución earthquake of 25 March 2012 in its context. At the top we show a simplified version of the slip distribution of the Maule 2012 mega earthquake determined by Ruiz et al. (2012). At the bottom we show an expanded map of the region of the 2012 Constitución earthquake. The red and blue stars are the *epicenters* of the 2012 earthquake computed using the P_1 and P_2 waves, respectively. The small green dots are the aftershocks of Constitución 2012 earthquakes located by SSN. The diamonds are the high-rate GPS stations and the GO05 accelerograph. The rupture area of the Talca 1928 earthquake is indicated by the thick black line. Other historical events are indicated by ellipses. (For interpretation of the references to color in this figure legend, the reader is referred to the web version of this article.)

1 December 1928 (although the location, the depth and dimension of the latter are constrained only by seismic intensities and a few teleseismic records; see Beck et al., 1998). The Constitución earthquake appears to bridge a gap at ∼35°S between the area of maximum slip during the Maule earthquake in the shallow part of the fault plane (>15 m of slip at a depth close to 15 km) (Ruiz et al., 2012 and references therein) and a deeper region of the subduction interface at depths greater than 45 km where more than 60 cm of afterslip occurred in the 12 days following the earthquake (Tong et al., 2010; Vigny et al., 2011). A seismic marine profile (Moscoso et al., 2011), as well as detailed models of the slab geometry (Hayes et al., 2012; Tassara et al., 2006), suggest that the dip of the plate interface between the Nazca and South American plates at 35°S is close to 10°–12° down to at least 25 km depth. At greater depth (40–50 km), seismicity reported for a temporary passive seismic network and aftershocks of the Maule earthquake indicate a steeper dip of 28° (Dannowski et al., 2013;

Lange et al., 2012). The hypocenter of the 2012 Constitución earthquake was located in that steeper and deeper part of the plate interface, at depths that are similar to that of the Mw 7.7, 2007 Tocopilla earthquake that only broke the deeper part of seismogenic zones in northern Chile, several hundred kilometers to the north of the Maule earthquake (Contreras-Reyes et al., 2012; Fuenzalida et al., 2013 and reference herein).

The 2012 Constitución earthquake was recorded by high-rate GPS stations, local seismometers and accelerometers, and by the Global Seismographic Network (GSN). We used these data together with InSAR images to perform kinematic inversions of the Constitución earthquake, to study its rupture nucleation and propagation, and to determine the location of slip within the seismogenic contact zone. Our results provide a precise location of this Mw 7.0 interplate thrust aftershock in a place that has repeatedly broken in recent history – in 1928 and 2010.

2. Data

The 2012 Constitución earthquake was well recorded by a network of high-rate GPS stations operated by Universidad de Chile and Universidad de Concepcion in Chile, École Normale Supérieure and Institut de Physique du Globe de Paris in France and the Geoforschung Zentrum (GFZ) of Potsdam, Germany (Fig. 1). The National Seismological Service of Universidad de Chile (SSN) has a regional network composed of accelerometers, broadband and short-period instruments that also recorded the main event and its aftershocks. In addition, broadband seismometers of the GSN recorded the mainshock at teleseismic distances. Finally, Synthetic Aperture Radar (SAR) data were acquired prior to and after the earthquake by European Space Agency's ENVISAT satellite.

3. Nucleation

Several well-recorded Chilean interplate thrust earthquakes have had very distinct nucleation phases observed before the arrival of the main phase from the hypocenter of the event. For instance, the 1985 Valparaíso earthquake had a clear 10 s nucleation phase (Korrat and Madariaga, 1986; Choy and Dewey, 1988), while the Tocopilla 2007 earthquake had a short nucleation phase that lasted only 0.5 s (Ruiz et al., 2011). Finally the Maule 2010 earthquake had a high frequency nucleation phase that preceded the main low frequency P wave by several seconds (Vigny et al., 2011). To better identify the nucleation process of the Constitución 2012 earthquake, we made a stack of unfiltered teleseismic records of the USArray Backbone network (Fig. 2). Fig. 2B shows that the nucleation phase lasted about 6 s. The same nucleation time is observed in the strong motion record of station GO05 located near the epicenter (see location in Fig. 1). Fig. 3 shows the ground velocity record from this station, in which the main P wave starts about 6 s after the first P wave arrival. Using available regional records, we located the first P wave (P_1) and the main P wave (P_2). The hypocenter of the 25 March 2012 Constitución earthquake (P_1) was located by SSN at 35.20°S, 72.22°W and 40.7 km depth, and by USGS at 35.18°S, 71.79°W and 34.8 km depth. These two locations differ by about 50 km, a common occurrence in Chile because USGS does not use local stations for their preliminary locations. Our relocation of the initial P_1 phase places the hypocenter at 35.298°S, 72.10°W and 39 km depth (22:37:7.02 UT), only a few km away from the SSN hypocenter. We then relocated the origin of the main P phase, P_2, at 35.24°S, 72.21°W and 39 km depth (22:37:13.20 UT). We do not have a very good control on depth, because it was not possible to pick the P_2 wave in all the records. The P_2 hypocenter is located to the west of P_1, closer to the gCMT centroid located at 35.31°S and
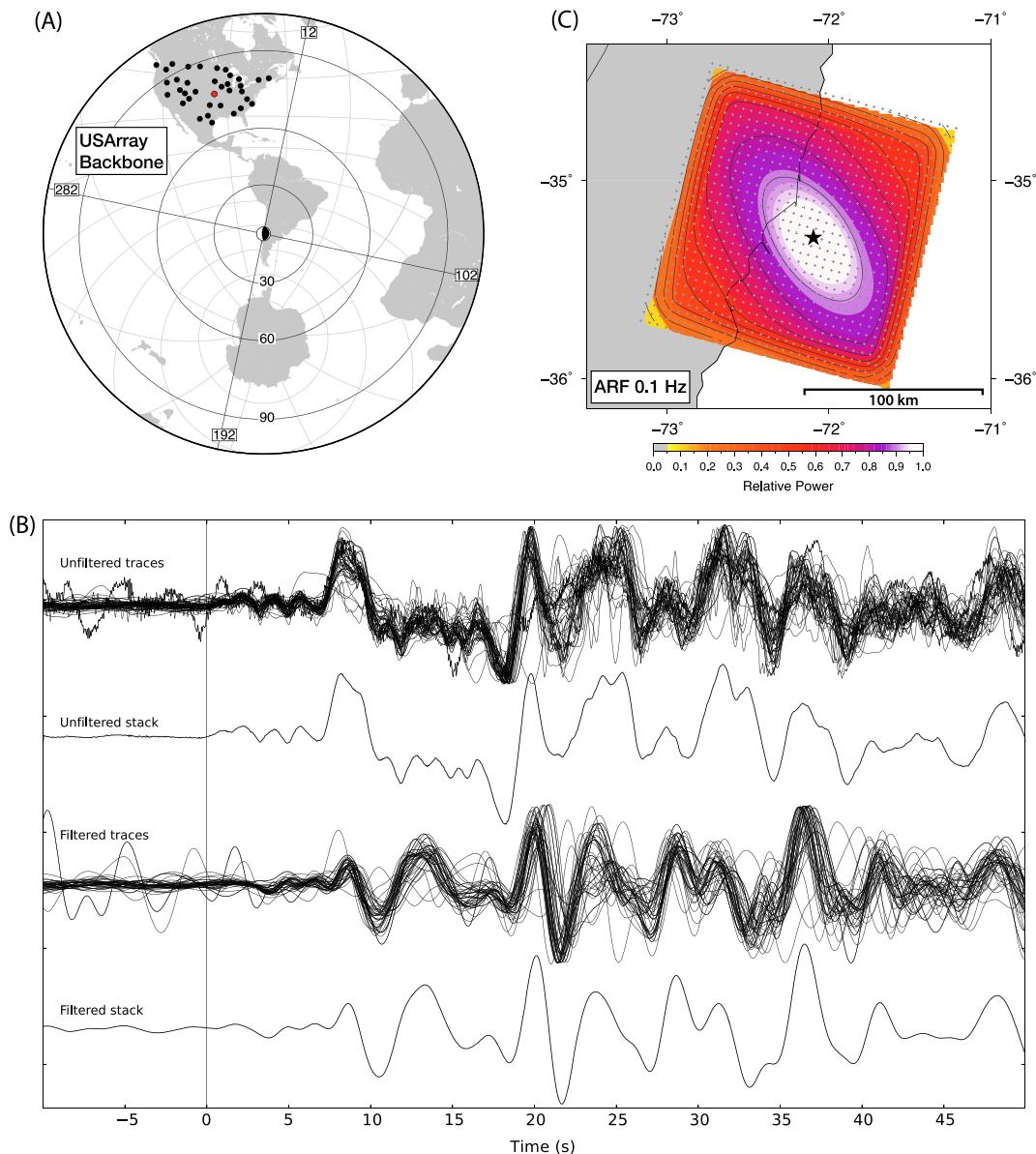
Fig. 2. The Constitución earthquake of 25 March 2012 as seen from North America (A) Map of the USArray Backbone network, used to identify the nucleation phase and for the back projection analysis (see Fig. 7). (B) The first 50 s of the P wave signal recorded at vertical components realigned according to the first P arrival. First two plots (from top to bottom) show the unfiltered traces and their associated stack. The last two plots show the traces filtered between 0.1 and 0.5 Hz and their associated stack. Note the ∼6 s nucleation phase in the unfiltered stack. (C) Array Response Function (ARF) of the station configuration at 0.1 Hz, calculated for a synthetic source located at the first hypocenter. (For interpretation of the references to color in this figure, the reader is referred to the web version of this article.)

72.41°W and 33.82 km, suggesting that P_2 is the initiation of the main moment release.

4. Earthquake modeling

In our inversions we used the proposed hypocenter for the P_1 phase relocated at 35.29°S, 72.10°W, with an origin time of 22:37:7.02 UT on 25 March 2012, and a depth of 39 km. We used the focal mechanism proposed by the USGS Centroid Moment Solution (strike = 12°, dip = 19°, rake = 101°). For the teleseismic and cGPS inversion we used the velocity models proposed for this region by Campos et al. (2002). For teleseismic, cGPS and joint GPS and InSAR inversions we assumed a fault plane of 80 km by 80 km, with the orientation of the USGS focal mechanism. The coordinates of the middle of the upper edge of the dislocation are (72.7°W; 35.1°S; 19 km depth) (see Supplementary Fig. S1).

4.1. Teleseismic kinematic slip inversion

We inverted teleseismic P and SH waves using the approach of Kikuchi and Kanamori (1991). We used 40 P-phases and 6 SH-phases, recorded by broadband stations of the GSN located between 30° and 100° from the epicenter in order to avoid upper mantle phases. The P and SH wave signals were windowed and filtered between 0.002 and 0.5 Hz and then integrated to displacement. The proposed fault plane model was subdivided into 16 by 16 subfaults. Rupture was modeled by a circular rupture front propagating at 2.2 km/s. We tested inversions with the rupture velocity varying from 1.2 to 2.7 km/s, at 0.5 km/s increments, and found similar results (see Supplementary Fig. S2). The lowest variance was obtained for a rupture velocity $V_r = 2.2$ km/s, which is also consistent with the relative timing and distance between first (P_1) and second (P_2) hypocenter. The moment rate (source time) function for each subfault was modeled by 4 triangular functions
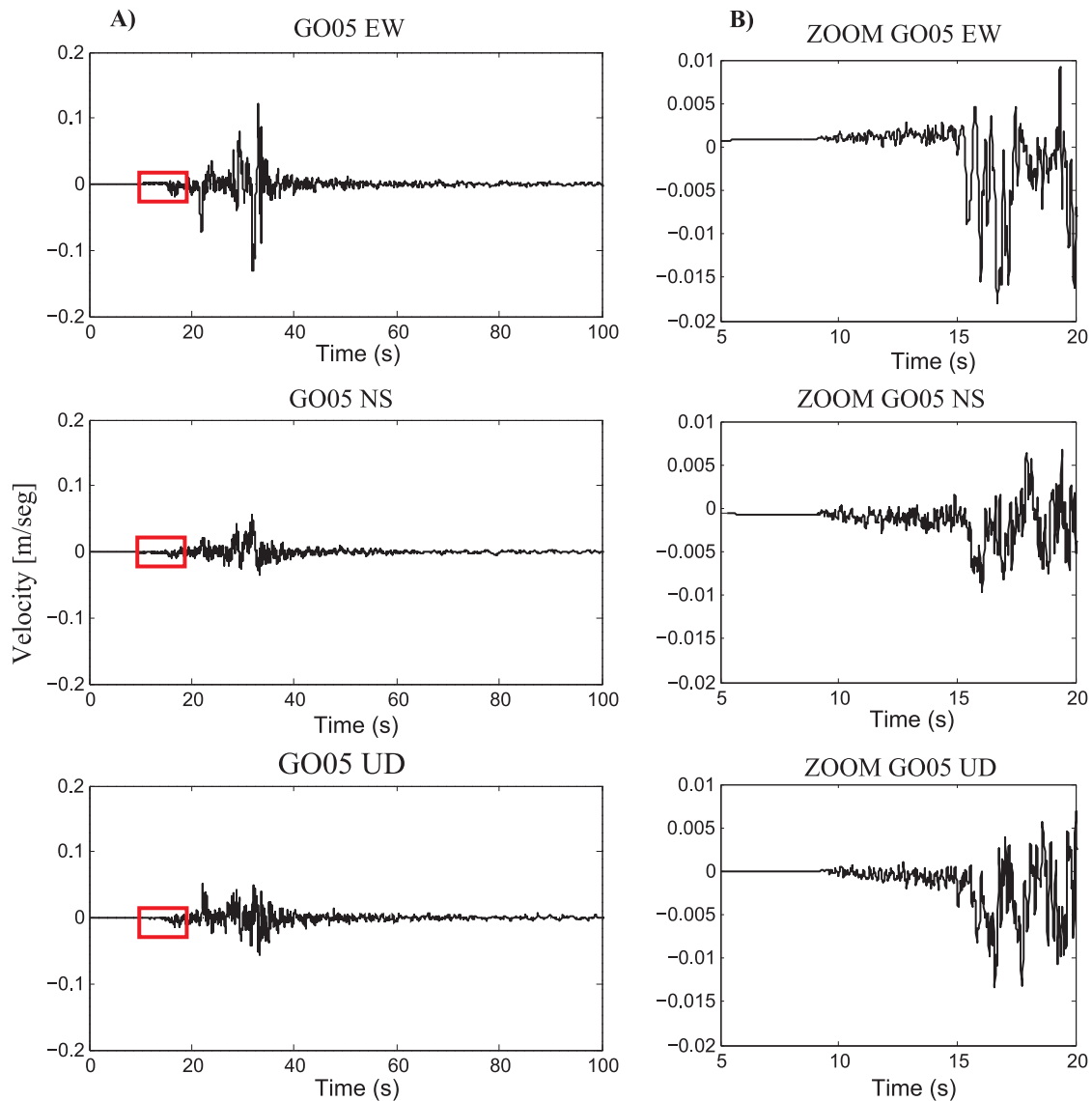
Fig. 3. The Constitución earthquake of 25 March 2012 at regional distances. Plots show the three component strong motion record at the GO05 station, integrated once to obtain velocities. (A) Full record, showing S_1 and S_2 arrivals; color boxes indicate the portion of signal that is shown in (B). (B) Zoom of velocity records shown in (A), the main P wave (P_2) arrives 6 s after the first P wave (P_1). Note that the P_1 wave is almost nodal because the auxiliary fault plane of the earthquake is very close to the location of the GO05 station.

of 4 s duration, overlapping for 2 s, for a total of 10 s possible total rupture duration.

The results of the teleseismic waveform inversion are shown in Fig. 4, while Fig. 5 shows the observed and synthetic waveforms and the distribution of the stations used in this analysis. The total seismic moment is 4.28×10^{19} Nm (Mw = 7.02) and the maximum slip is about 2 m, assuming a rigidity of 50.4 GPa derived from the velocity model of Campos et al. (2002).

4.2. Back projection analysis

We studied the short-period radiation from the Constitución earthquake using a back projection (BP) algorithm applied to teleseismic P wave recordings, following the method proposed by Satriano et al. (2012). We used vertical components of the USArray Backbone network (Fig. 2A), filtered between 0.1 and 0.5 Hz. As shown in Fig. 2B, in this frequency band the signal is sufficiently similar across the network that it is possible to exploit amplitude and/or phase coherency for the BP analysis. The first 6 s of the nucleation phase have significantly smaller amplitude (about three

times) with respect to the later arrivals. To avoid the later arrivals dominating the BP results, we chose to apply a one-bit normalization (e.g., Derode et al., 1999) to the traces in order to retain only phase information. Sources of coherent short-period radiation are searched on a grid of 170 by 140 km, with square cells of 5 km on each side; the grid depth was fixed at 35 km.

The results of the BP analysis are presented in Fig. 6. Fig. 6A shows the spatial distribution of maximum power of the one-bit stack, computed at each node of the grid during the rupture, as interpolated surface and contour lines. This image has to be compared with the array response function (ARF) of the station configuration, shown in Fig. 2C for a frequency of 0.1 Hz, to understand the resolvable extent of high frequency radiation. The area of maximum stack power is appreciably more extended than the resolution spot in the E–W, direction and is shifted towards the NW, indicating that the rupture extended up-dip with respect to the nucleation hypocenter. Fig. 6B shows the spatio-temporal distribution of BP peaks, with amplitude proportional to the relative BP power of the one-bit stack, and color indicating relative time after the P_1 nucleation phase. During a first stage, which lasted about
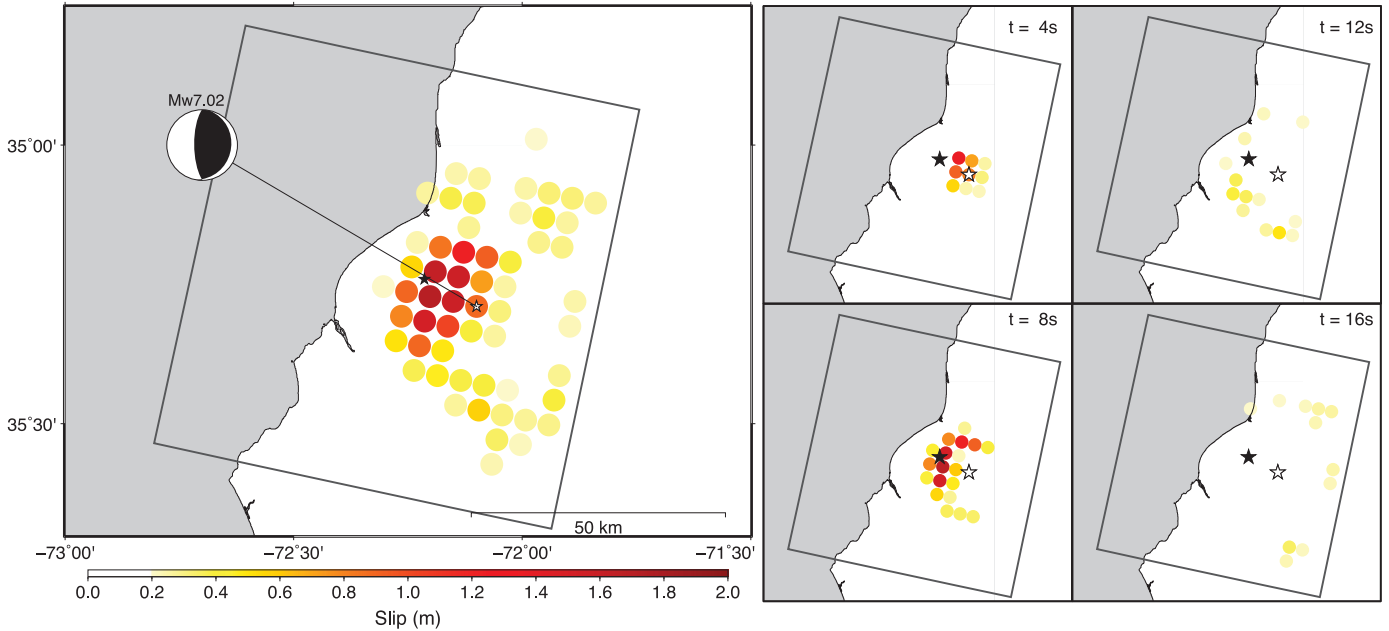
Fig. 4. Finite source model of the 2012 Constitución earthquake from teleseismic inversion. (Left) Slip distribution on the fault, white and black stars indicate the P_1 and P_2 hypocenters, respectively. Black square represents the fault plane for calculating synthetic waveforms. (Right) Snapshots of the rupture propagation at 4 s intervals derived from teleseismic inversion. The slip release during each interval is shown using the color scale of the left plot. (For interpretation of the references to color in this figure legend, the reader is referred to the web version of this article.)

20 s, the source of radiation remains close to the hypocenter (for about 13 s), and then moves northwards, up to ∼35 km away from the nucleation point. We interpret this northwards propagation as a distortion effect due to the constructive interference of depth phases, which produce a bias in back projection images (Yagi et al., 2012; Yao et al., 2012). To support this interpretation, we modeled the P–pP–sP wave train associated to the P_2 hypocenter at one central station of the US network (KSU1 – shown in red on Fig. 2A), and we compared the timing of the northwards-trending peaks with the arrival time of pP and sP phases. pP and sP arrivals form the P_2 hypocenter correspond to the BP peaks between 14 and 20 s (see Supplementary Figs. S3 and S4). Those peaks are therefore dimmed out in Fig. 6 and will not be discussed. In a second stage, starting about 20 s from the earthquake origin, short-period energy is radiated close to the P_2 hypocenter and then propagates towards the NW, in the up-dip direction.

4.3. Kinematic inversion of high-rate GPS records

We also performed a regional source inversion using all available high-rate GPS and strong motion records. The CONS cGPS record and the GO05 strong motion record were filtered using a low pass Butterworth causal filter with 0.5 Hz cut-off frequency. Only the static displacements at ILOC, PELL, NRVL, CAUQ and MAUL cGPS records were inverted, because they have low signal to noise ratio in the high frequency range (0.1 to 0.5 Hz). We inverted for a simple elliptical rupture patch for the kinematic inversion since the near field data is sparse (Vallée and Bouchon, 2004; Ruiz and Madariaga, 2011; Ruiz et al., 2012). The elliptical patch is located inside the proposed fault plane model subdivided into 20×20 subfaults. We assumed that slip has a Gaussian distribution:

$$D(x, y) = D_m \exp\left[-\left(\frac{x^2}{a^2} + \frac{y^2}{b^2}\right)\right] \qquad (1)$$

where D_m is the maximum amplitude of slip inside the elliptical patch of semi-axes a and b. During the inversion, we also inverted for the rupture velocity V_r. However, since we used only

two complete seismograms (GO05 and CONS) we do not have a good control on V_r. We obtained low misfits for V_r in the range from 2.5 to 3.0 km/s; the best solution has $V_r = 2.6$ km/s. The source time function was the same for every point on the fault. By trial and error, we chose a triangular function of duration 1 s around the rupture time. The AXITRA code (Coutant, 1990; Bouchon, 1981) was used to simulate wave propagation from the source to the receivers using the velocity structure proposed by Campos et al. (2002). Synthetic records were compared with real records, using a normalized $L2$ norm. The solution (Fig. 7) shows that rupture propagated from the hypocenter towards the west, or from hypocenter (P_1) towards the centroid. Comparisons between observed and synthetic records are shown in Fig. 8. The maximum slip D_m is 2.3 m, the semi-axes $a = 11.2$ km and $b = 15.4$ km and the moment obtained is 4.64×10^{19} Nm (Mw 7.04), assuming a rigidity of 50.4 GPa, in very good agreement with the moment retrieved from the teleseismic inversion.

4.4. InSAR modeling

Systematic SAR acquisitions by the ENVISAT satellite in Central Chile have been requested since 2010, with the intention of monitoring the post-seismic activity following the Maule earthquake, including significant aftershocks. In order to cope with dwindling fuel resources and allow for extension of the duration of the mission, the spacecraft was shifted to a drifting orbital configuration since October 2010, leaving only the ascending orbits available for SAR interferometry (InSAR) at the latitude of Central Chile. ENVISAT was eventually lost 14 days after the Constitución earthquake (on 8 April 2012), after 10 years of service. Fortunately, an acquisition was performed 11 days after the earthquake (on 5 April 2012). In combination with another acquisition 19 days before the earthquake on 6 March 2012, we computed an interferometric measurement of the ground deformation associated with the earthquake. DORIS precise orbits and the SRTM DEM were used for orbital and topographic InSAR corrections, respectively. The InSAR data were calculated with the ROI_PAC software (Rosen et al., 2004). Despite the 260 m perpendicular baseline,
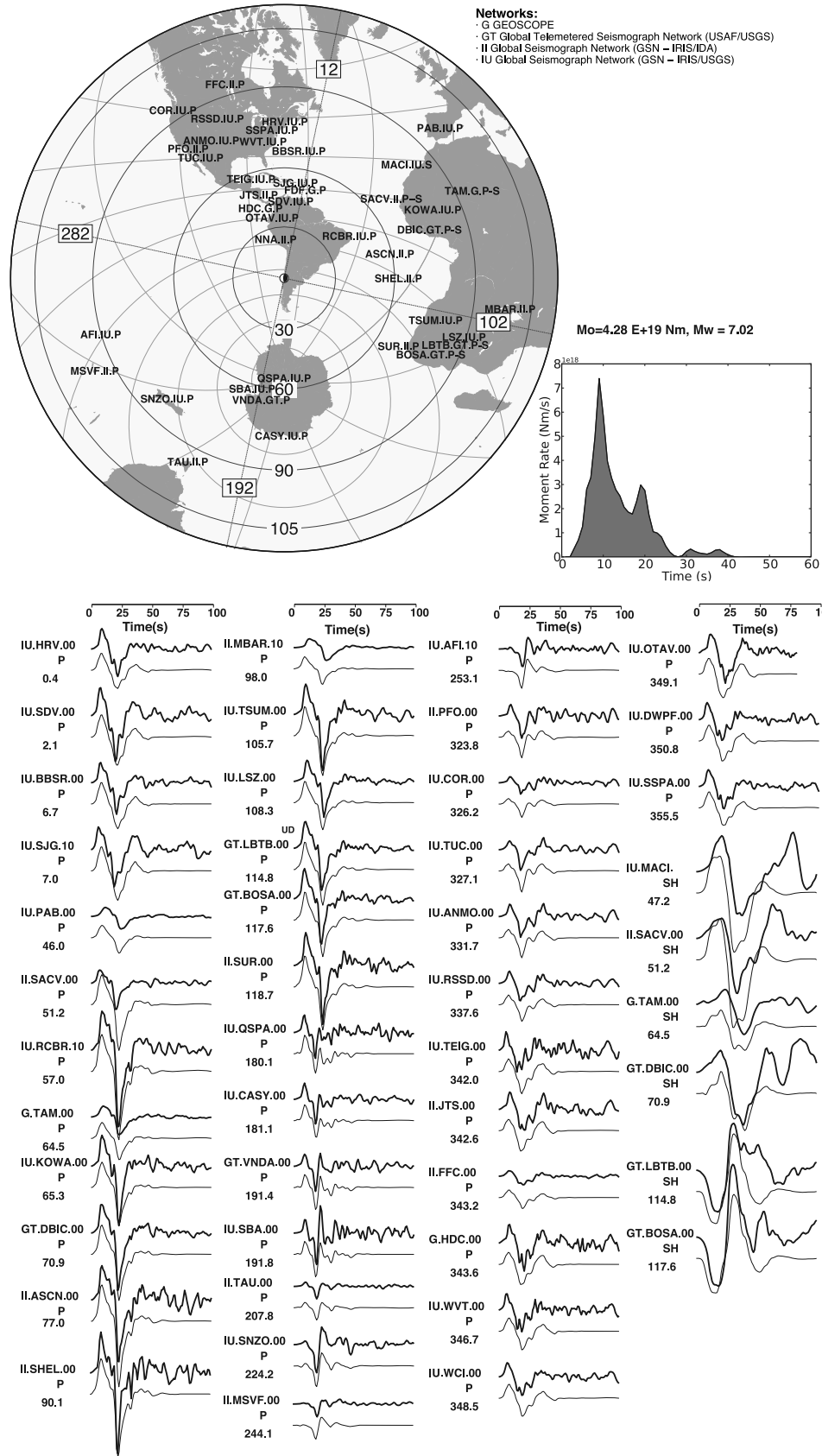
Fig. 5. Observed and simulated P and S waveforms for the teleseismic inversion of the 25 March 2012 Constitución earthquake. Stations used in the inversion are displayed (top figure), with observed and synthetic waveforms shown as thick (top) and thin (lower) lines, respectively (bottom figure). The letter and the number below station code are phase type and azimuth in degrees, respectively; the scale the waveforms is time in seconds. Distribution of stations, with black circles representing epicentral distances between 30° and 105° from the mainshock, the epicenter is represented by its focal mechanism. The moment rate function is on the right of the station map.
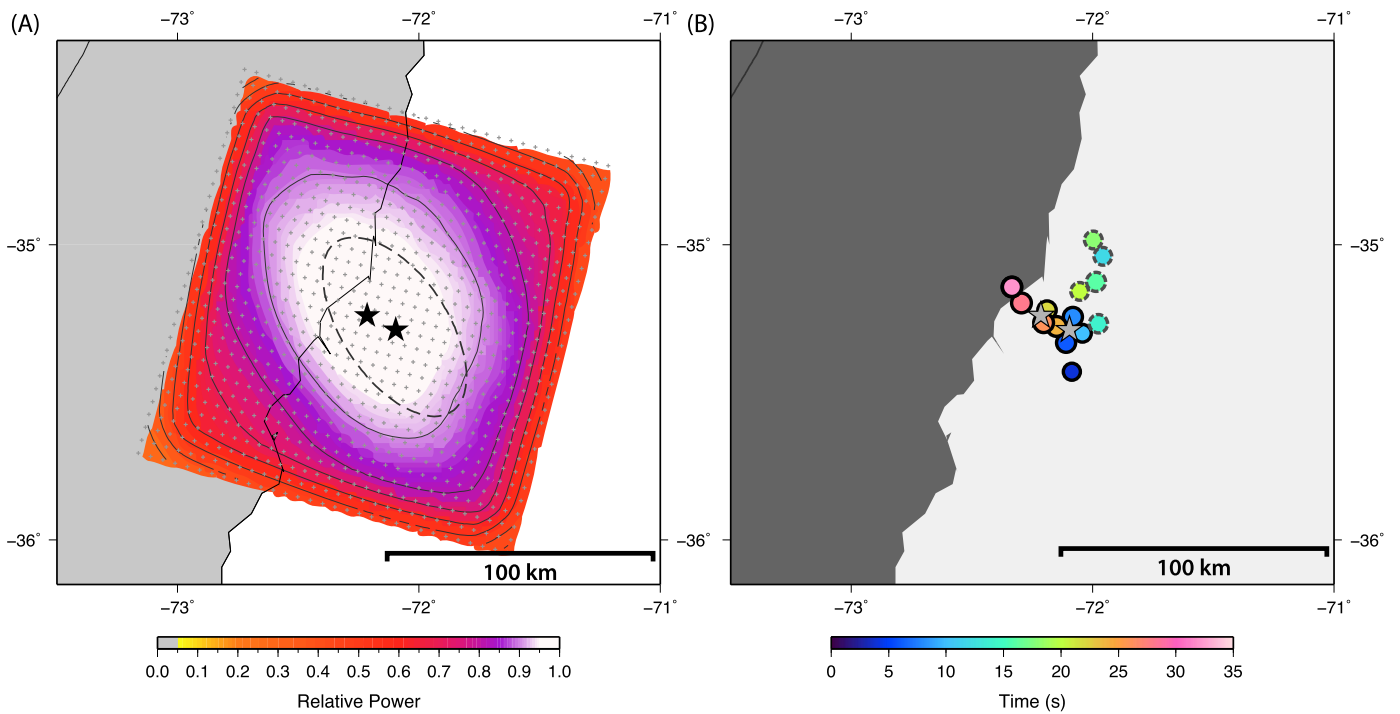
Fig. 6. Back projection of the 25 March 2012 Constitución earthquake. (A) Normalized maximum radiated power in the frequency band 0.1–0.5 Hz. The two stars are the epicenters derived from the P_1 and P_2 phases, respectively (see Fig. 1). Grid nodes are indicated by gray dots. Dashed line is the 90% contour of the ARF (see Fig. 2C). (B) Back projection peaks colored by elapsed time since the onset of the P_1 phase, and scaled by stack amplitude.
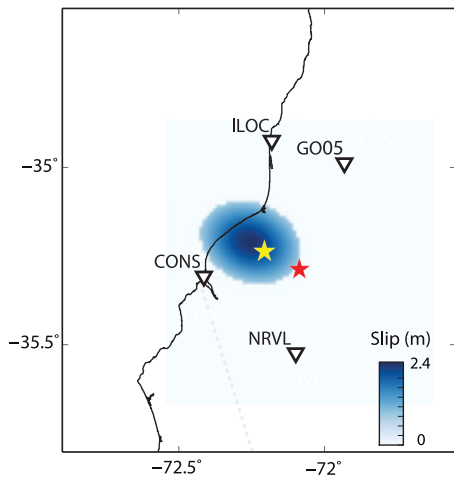

Fig. 7. Slip distribution of the Mw 7.0 Constitución earthquake of 25 March 2012 obtained from the inversion of the GO05 accelerogram, high-rate GPS records and static GPS vectors. The rupture starts at the epicenter shown by the red star, and propagates in the northwest direction; the maximum slip is concentrated in the zone where the main P and S waves (P_2 and S_2) were generated. (For interpretation of the references to color in this figure legend, the reader is referred to the web version of this article.)

the interferogram has a good coherence. After phase unwrapping, a residual topography-correlated, presumably tropospheric component was subtracted empirically by determining a linear relationship between phase and elevation in areas of the interferogram obviously not affected by appreciable tectonic deformation, and by extrapolating this relation to the coastal area.

The interferogram is shown in Fig. 9. Due to the incidence angle of the line-of-sight (LOS) with respect to the vertical (35° on average), the satellite is most sensitive to vertical displacement. A maximum LOS displacement of 12 cm towards the satellite oc-
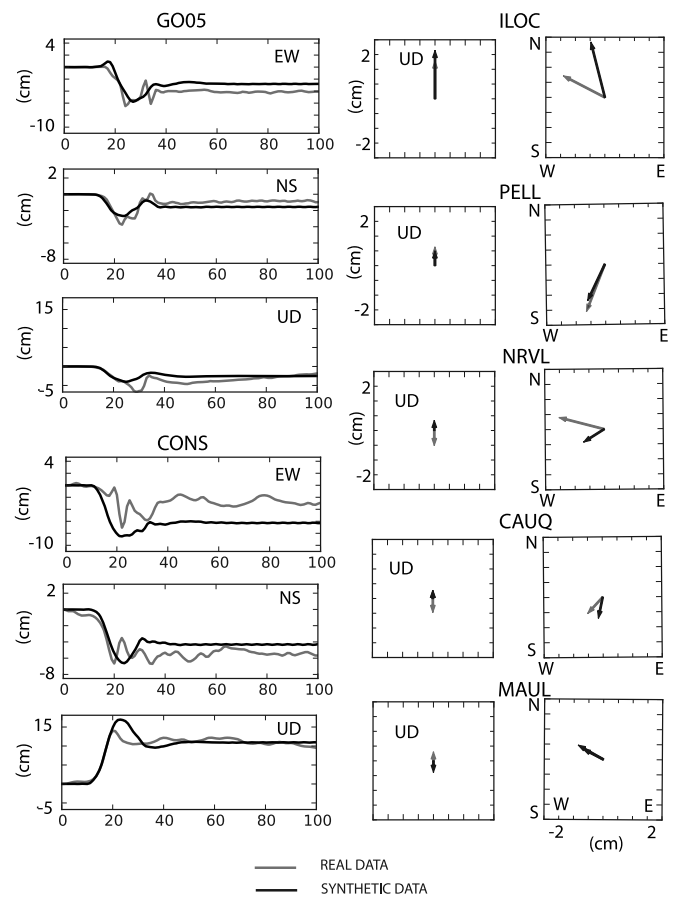

Fig. 8. Near field displacement data for the Mw 7.0 Constitución earthquake of 25 March 2012: Comparison of real and synthetic displacement records. (A) GO05 strong motion and CONS cGPS record. (B) GPS displacement vectors from the GOPS stations plotted in Fig. 1B.
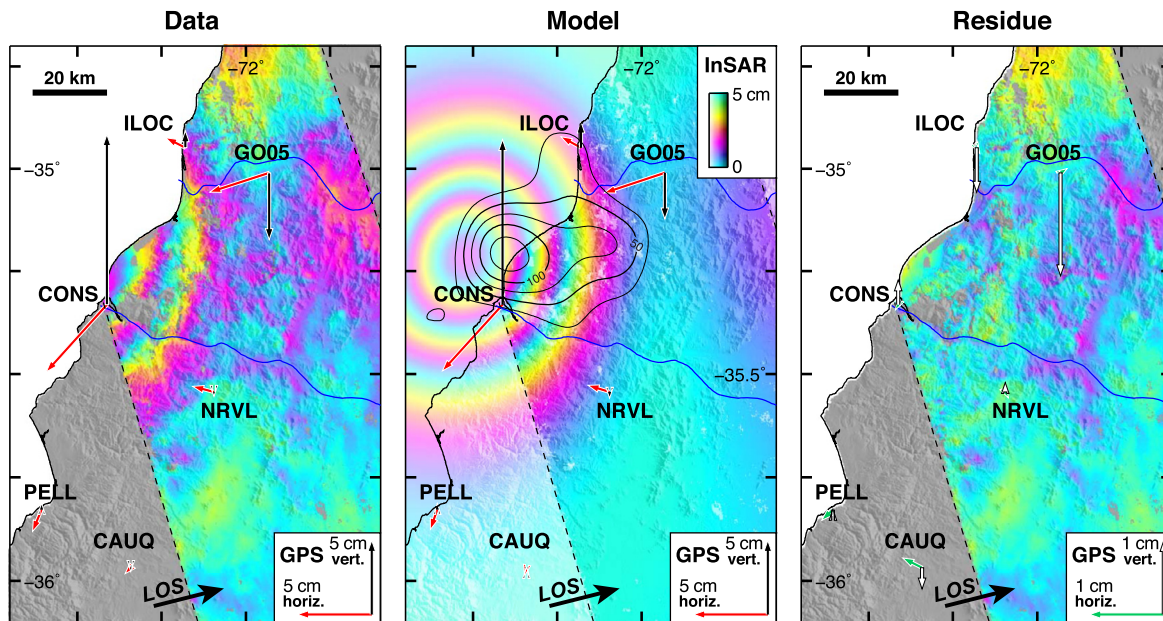
Fig. 9. Surface deformation due to the 2012 Constitución earthquake determined by InSAR, static GPS and integrated strong motion data. The left panel shows the measured displacement, the middle panel shows the synthetic displacements computed from inversion of the geodetic data; superposed on this image we plot the contour lines of slip for the inverted model. The right panel shows the residues. Vertical and horizontal GPS vectors are indicated by the arrows. Note that a different scaling of the GPS vectors is used in the right panel. Color cycles correspond the line-of-sight (LOS) component of the ground displacement derived from InSAR. Positive LOS displacement indicates motion towards the satellite. (For interpretation of the references to color in this figure legend, the reader is referred to the web version of this article.)

curs at the location of the city of Constitución, in agreement with the modulus and direction of the static displacement vector measured at GPS station CONS.

4.5. Joint inversion of InSAR data and GPS records

Finally, we inverted jointly the InSAR data, the displacement vectors retrieved from six GPS stations with well-constrained static offsets (CAUQ, CONS, ILOC, MAUL, NRVL, PELL), and the static offset vector obtained by double integration of the accelerogram recorded at station GO05. Prior to the inversion, the InSAR data were decimated, using a decimation factor increasing as the distance from the epicenter (Grandin et al., 2009). The number of InSAR data used in the inversion was kept relatively small (97) so that the GPS data (18 components) and accelerometric data (3 components) weight significantly on the inversion result. Relative weighting between the data sets also depends on the assumed uncertainty affecting each measurement. The assumed values of 0.5 cm for InSAR data, 0.05 cm for horizontal GPS data and 0.1 cm for vertical GPS data were chosen to achieve a compromise between a purely InSAR-dominated and a purely GPS-dominated inversion. Uncertainty within the InSAR data was assumed to be uncorrelated (no data covariance).

The inversion procedure is similar to that used by Jónsson et al. (2002). The fault was assumed to be embedded in an elastic half space of Poisson's ratio equal to 0.25. The proposed fault plane was discretized into a series of contiguous rectangular dislocations of 5 by 5 km. Green's functions were computed using Okada's (1985) formulas. The parameters controlling the fault geometry and slip direction (strike, dip, rake) were fixed according to the USGS centroid moment solution. The depth of the fault plane was adjusted so that the patch lying nearest to the hypocenter has a depth of 39 km. A least-square inversion including a non-negative slip constraint was implemented. We used Laplacian smoothing, with the value of the regularization parameter chosen using an L-curve trade off criterion. Zero-slip boundary conditions on the fault edge were adopted.

The best slip solution that we obtained is shown in Fig. 9 and Fig. 10a. The fit to the InSAR data is generally excellent, with maximum LOS displacement misfit smaller than 1 cm. The reduction of the root mean square GPS displacement is 87%, with residuals generally smaller than 0.5 cm. The largest misfit is found for the vertical component of the strong motion station GO05 (1.3 cm). We attribute this misfit to the effect of noise amplification resulting from double integration of the GO05 accelerogram.

Our best model has a total geodetic moment is 6.66×10^{19} Nm (Mw = 7.15 assuming a modulus of rigidity of 50.4 GPa). Peak slip is within the range of 1.2–3.0 m, depending on the amount of smoothing imposed in the inversion (see Supplementary Fig. S5). In contrast, the area of significant slip (>50 cm), with a radius of 20 km, depends very little on the choice of the smoothing parameter. Since geodetic measurements are located onshore, the data resolution tends to decrease offshore. This could lead to a poor estimation of slip occurring trench-wards from the coast. Nevertheless, resolution and restitution tests (see Supplementary Material) indicate that any slip occurring within 20 km from the coast is resolvable by the data. Furthermore, the agreement between the total moment determined independently by the geodetic data and the seismic data suggests that slip occurring beyond 20 km distance from the coast, if any, is likely to be modest. Peak slip, which roughly coincides with the centroid, appears to be located right beneath the coastline, 10–15 km to the north–north-east of the city of Constitución. For comparison, the centroid of the 2010 Maule earthquake was located offshore, 50–75 km to the south-west of the city of Constitución (Vigny et al., 2011). The down-dip location of the 2012 event with respect to the 2010 event is well constrained by the strikingly different behavior of GPS station CONS, which subsided by 37 cm during the 2010 Maule earthquake, and was uplifted by 12 cm during the 2012 Constitución earthquake.

5. Discussion

We studied the 25 March 2012 aftershock of the 2010 Maule earthquake with a variety of seismic and geodetic data. With these data we determined that the earthquake ruptured the deeper part
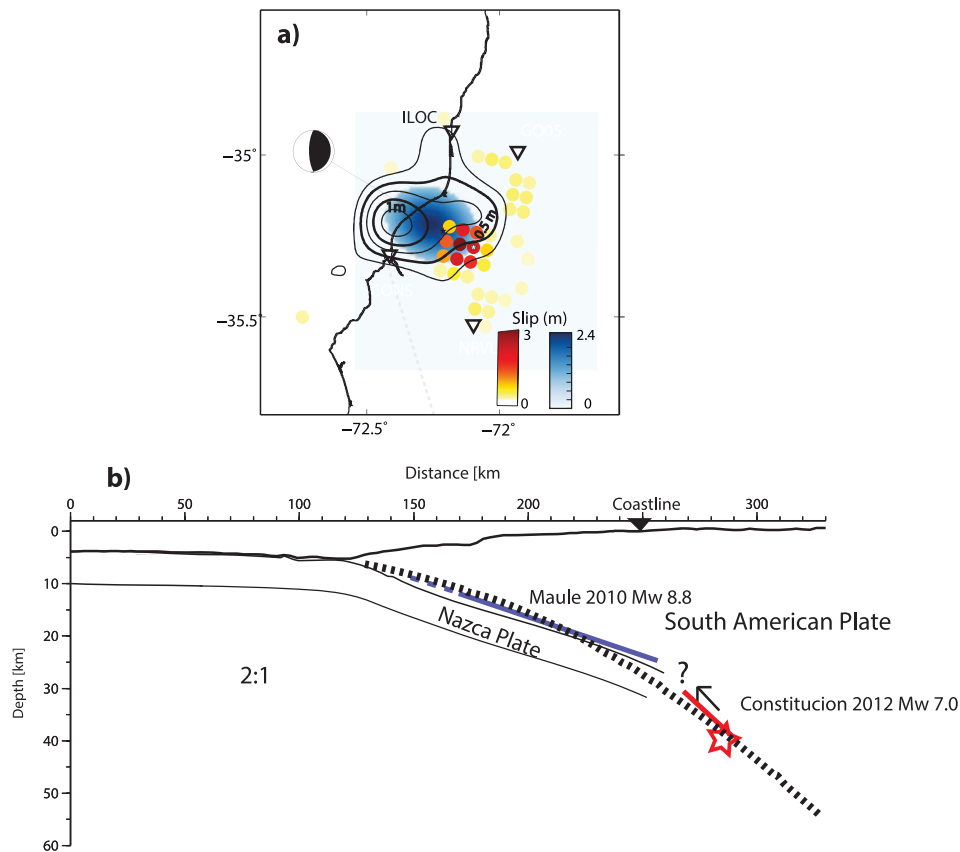
Fig. 10. (a) Slip distribution obtained from teleseismic records (color dots), together with InSAR images and GPS data (contour lines) and from GPS and strong motion records (gray shading). Color and gray scales are saturated to 4 m. (b) Geometry of the subducting Nazca plate modified from Moscoso et al. (2011) (black line). The black dashed line is the geometry of the slab interface proposed by Hayes et al. (2012). The thick blue line shows the Maule 2010 rupture zone (Ruiz et al., 2012). Red line is the Constitución 2012 rupture zone; red star is the hypocenter derived from P_1 waves (2:1/V:H scale). (For interpretation of the references to color in this figure legend, the reader is referred to the web version of this article.)

of the interface between the Nazca and South American plates near the city of Constitución at 35.5°S. The earthquake began with a low amplitude nucleation phase at about 40 km depth, then waited about 6 s, and finally triggered the main rupture from the centroid of the event situated approximately 10 km up-dip from the initial shock. The largest P wave phase observed in the seismograms – which we called the P_2 phase – was radiated from the vicinity of the centroid determined by the USGS centroid moment solution. The seismic moment determined by different data sets varies between $Mo \sim 4.6 \times 10^{19}$ Nm (from teleseismic and GPS inversion) to $Mo \sim 6.7 \times 10^{19}$ Nm (from InSAR and GPS inversion), confirming that our results are robust.

The 2012 event is one of the largest thrust aftershocks of the Maule mega-thrust earthquake, together with the Mw 7.2 event of 2 January 2011, near the southern end of the rupture zone. The other large aftershocks of the Maule earthquake were two shallow normal fault aftershocks of 11 March 2010 (Mw 7.0 and Mw 6.9) and a large outer rise event of Mw 7.4 that occurred on 27 February 2010, a few hours after the main event. It appears, then, that the Maule mega-thrust earthquake has not caused as many large plate interface aftershocks as are typically expected from the so-called Bath's (1965) rule that states that the largest aftershock has 1.2 magnitude units less than that of the mainshock. A possible explanation for this lack of interplate aftershocks is that the aftershock series is not yet complete. An alternative explanation is that the Maule earthquake, like other mega-thrust earthquakes, broke the shallow part of the plate interface that ruptures smoothly, as proposed by numerous authors after the Tohoku earthquake (e.g., Lay et al., 2012; Yao et al., 2013). Moscoso et al. (2011) found

from marine geophysics reflection profiles that the shallow part of Nazca plate interface near 35°S has a very low dip angle, between 10° and 12°. This is quite different to the 19° dip of the focal mechanism of the 2012 Constitución earthquake determined from USGS centroid moment tensor, the 16° dip determined by gCMT and the 18° dip of the USGS W-phase solution. Since the earthquake occurred at a depth of 40 km under the coast of central Chile, this geometry difference implies that there should be a bend in the plate interface about 100 km from the trench at depths close to 20–25 km (Fig. 10b). This inferred bend may be similar to that observed in northern Chile by Contreras-Reyes et al. (2012) and by Fuenzalida et al. (2013). A substantial data set of aftershocks of the Maule 2010 earthquake has been recently reported by Lange et al. (2012) and Rietbrock et al. (2012). These aftershock catalogs show good correlation with regionally and teleseismically determined slab models. However, more detailed relocation work is necessary to determine the depth of the aftershocks located in the shallower part of the plate interface (Fuenzalida, 2013). Most Chilean thrust earthquakes of magnitude greater than 7.4 have focal mechanisms with dip angles of 20°, on average as shown in Table 1.

All these events broke the deeper areas of the plate interface. It is tempting then to follow the reasoning of Lay et al. (2012) and propose that most Mw $\sim$8.0 events in Chile occur along the deeper part of the plate interface. There are some exceptions; for example the series of shallow thrust events that occurred south of Coquimbo in north-central Chile (30°–31°S) in July 1997 (see Lemoine et al., 2001; Pardo et al., 2002; Gardi et al., 2006) broke the plate interface near the center of the seismogenic zone

Table 1
Dip angle of most Chilean thrust earthquakes of magnitude greater than 7.4.

Earthquake	Magnitude	Dip	Reference
01/12/1928	Mw 7.9	20°–30°	Beck et al. (1998)
28/12/1966	Mw 7.7	41	Malgrange and Madariaga (1983)
21/12/1967	Mw 7.4	28	Malgrange and Madariaga (1983)
09/07/1971	Mw 7.8	66	Malgrange and Madariaga (1983)
04/10/1983	Mw 7.6	20	gCMT
03/03/1985	Mw 7.9	26	gCMT
30/07/1995	Mw 8.0	22	gCMT
14/11/2007	Mw 7.7	20	gCMT

(15–25 km depth) and they eventually triggered the Mw 7.1 Puni-taqui intermediate depth "slap-push" event in October 1997. According to Métois et al. (2012), the Coquimbo area behaves very differently from the Maule segment, because GPS data shows that this region is only partially coupled. The Mw 8.1 Antofagasta earthquake of July 1995 was initially reported to have broken the entire plate interface by Ihmlé and Ruegg (1997), who used teleseismic body waves and GPS vectors to define the rupture zone. Later aftershock data reported by Husen et al. (1999) showed that only the deeper part of the plate interface, below 20 km, broke during that event. This was later confirmed by aftershock relocations obtained by cross-correlation methods by Nippress and Rietbrock (2007). Thus, it appears that, with a few exceptions, most earthquakes with Mw close to 8.0 in Chile have broken only the deeper parts of the plate interface.

6. Conclusions

The Mw 7.0 25 of March 2012 Constitución earthquake is one of the largest interplate thrust aftershocks of 2010 Maule earthquake. The rupture of the 2012 earthquake has an area of roughly 10×20 km, and is located near the bottom of the seismogenic zone of the interface between the Nazca and South American plates. The Constitución earthquake has a complex initiation with a deep hypocenter at 39 km depth and a shallower main rupture. The latter coincides with the depth determined by moment tensor analysis. The earthquake occurred down-dip of the region of maximum co-seismic slip of the 2010 Maule earthquake, and up-dip of the region of rapid afterslip following that event. The nucleation phase of the 2012 earthquake lasted 6 s, which is unusually long for an earthquake of that magnitude (Ellsworth and Beroza, 1995). The different techniques used in this work produce consistent results, with up-dip propagation of the rupture from southeast to northwest. Fig. 10a summarizes the slip distribution proposed for the 25 March 2012 earthquake using teleseismic records, InSAR image, GPS data and strong motion records. We observed that the largest slip is concentrated in a zone of less than 20 km radius in the deeper part of the interface between the Nazca and South American plates, as sketched in Fig. 10b, where the location of Constitución 2012 rupture is compared with the Maule 2010 rupture.

Appendix A. Supplementary material

Supplementary material related to this article can be found online at http://dx.doi.org/10.1016/j.epsl.2013.07.017.

References

Astroza, M., Ruiz, S., Astroza, R., 2012. Damage assessment and seismic intensity analysis of the 2010 (Mw 8.8) Maule Earthquake. Earthq. Spectra 28 (S1), S145–S146.

Bath, M., 1965. Lateral inhomogeneities in the upper mantle. Tectonophysics 2, 483–514.

Beck, S., Barrientos, S., Kausel, E., Reyes, M., 1998. Source characteristics of historic earthquakes along the central Chile subduction zone. J. South Am. Earth Sci. 11, 115–129.

Bouchon, M., 1981. A simple method to calculate Greens functions for elastic layered media. Bull. Seismol. Soc. Am. 71, 959–971.

Campos, J., Hatzfeld, D., Madariaga, R., Lopez, G., Kausel, E., Zollo, A., Barrientos, S., Lyon-Caen, H., 2002. The 1835 seismic gap in South Central Chile. Phys. Earth Planet. Inter. 132, 177–195.

Choy, G., Dewey, J., 1988. Rupture process of an extended sequence: Tele-seismic analysis of the Chilean earthquake of March 3, 1985. J. Geophys. Res. 93, 1103–1118.

Contreras-Reyes, E., Jara, J., Grevemeyer, I., Ruiz, S., Carrizo, D., 2012. Abrupt change in the dip of the subducting plate beneath north Chile. Nat. Geosci. 5, 342–345, http://dx.doi.org/10.1038/ngeo1447.

Coutant, O., 1990. Programme de simulation numerique AXITRA. Rapport LGIT. Univ. Joseph Fourier, Grenoble, France.

Dannowski, A., Grevemeyer, I., Kraft, H.A., Arroyo, I., Thorwart, M., 2013. Crustal thickness and mantle wedge structure from receiver functions in the Chilean Maule region at 35°S. Tectonophysics 592, 159–164, http://dx.doi.org/10.1016/j.tecto.2013.02.015.

Derode, A., Tourin, A., Fink, M., 1999. Ultrasonic pulse compression with one-bit time reversal through multiple scattering. J. Appl. Phys. 85, 6343, http://dx.doi.org/10.1063/1.370136.

Ellsworth, W.L., Beroza, G.C., 1995. Seismic evidence for an earthquake nucleation phase. Science 268, 851–855.

Farías, M., Comte, D., Roecker, S., Carrizo, D., Pardo, M., 2011. Crustal extensional faulting triggered by the 2010 Chilean earthquake: The Pichilemu Seismic Sequence. Tectonics 30. TC6010, http://dx.doi.org/10.1029/2011TC002888.

Fuenzalida, A., 2013. Répliques des séismes de Tocopilla 2007 (Mw 7.6) et Maule 2010 (Mw8.8): Implications pour la subduction Chilienne. Thèse de Doctorat. ENS-IPGP, Paris, France.

Fuenzalida, A., Schurr, B., Lancieri, M., Sobiesiak, M., Madariaga, R., 2013. High-resolution relocation and mechanism of aftershocks of the 2007 Tocopilla (Chile) earthquake. Geophys. J. Int. 194 (2), 1216–1228, http://dx.doi.org/10.1093/gji/ggt163.

Gardi, A., Lemoine, A., Madariaga, R., Campos, J., 2006. Modeling of stress transfer in the Coquimbo region of central Chile. J. Geophys. Resi 111. B04307, http://dx.doi.org/10.1029/2004JB003440.

Grandin, R., Socquet, A., Binet, R., Klinger, Y., Jacques, E., de Chabalier, J.-B., King, G.C.P., Lasserre, C., Tait, S., Tapponnier, P., Delorme, A., Pinzuti, P., 2009. September 2005 Manda Hararo-Dabbahu rifting event, Afar (Ethiopia): Constraints provided by geodetic data. J. Geophys. Res. 114 (B8). CiteID B08404.

Hayes, G.P., Wald, D.J., Johnson, R.L., 2012. Slab1.0: A three-dimensional model of global subduction zone geometries. J. Geophys. Res. 117. B01302, http://dx.doi.org/10.1029/2011JB008524.

Husen, S., Kissling, E., Flueh, E., Asch, G., 1999. Accurate hypocentre determination in the seismogenic zone of the subducting Nazca Plate in northern Chile using a combined on-/offshore network. Geophys. J. Int. 138, 687–701.

Ihmlé, P.F., Ruegg, J.C., 1997. Source tomography by simulated annealing using broad-band surface waves and geodetic data: Application to the Mw = 8.1 Chile 1995 event. Geophys. J. Int. 131, 146–158.

Jónsson, S., Zebker, H., Segall, P., Amelung, F., 2002. Fault slip distribution of the 1999 Mw7.1 Hector Mine earthquake, California, estimated from satellite radar and GPS measurements. Bull. Seismol. Soc. Am. 92, 1377–1389.

Kikuchi, M., Kanamori, H., 1991. Inversion of complex body waves – III. Bull. Seismol. Soc. Am. 81, 2335–2350.

Korrat, I., Madariaga, R., 1986. Rupture of the Valparaíso (Chile) gap from 1971 to 1985. In: Das, S., Boatwright, J., Scholz, C.H. (Eds.), Earthquake Source Mechanics. AGU, Washington, DC, pp. 247–258.

Lange, D., Tilmann, F., Barrientos, S.E., Contreras-Reyes, E., Methe, P., Moreno, M., Heit, B., Agurto, H., Bernard, P., Vilotte, J.-P., Beck, S., 2012. Aftershock Seismicity of the 27 February 2010 Mw 8.8 Maule Earthquake Rupture Zone. Earth Planet. Sci. Lett. 317–318, 413–425.

Lay, T., Kanamori, H., Ammon, C.J., Koper, K.D., Hutko, A.R., Ye, L., Yue, H., Rushing, T.M., 2012. Depth-varying rupture properties of subduction zone megathrust faults. J. Geophys. Res. 117. B04311, http://dx.doi.org/10.1029/2011JB009133.

Lemoine, A., Campos, J., Madariaga, R., 2001. Evidence for earthquake interaction in the Illapel Gap of Central Chile. Geophys. Res. Lett. 28, 2743–2746.

Malgrange, M., Madariaga, R., 1983. Complex distribution of large thrust and normal fault earthquakes in the Chilean subduction zone. Geophys. J. R. Astron. Soc. 73 (2), 489–505.

Mendoza, C., Hartzell, S., Monfret, T., 1994. Wide-band analysis of the 3 March 1985 Central Chile earthquake: Overall source process and rupture history. Bull. Seismol. Soc. Am. 84 (2), 269–283.

Métois, M., Socquet, A., Vigny, C., 2012. Interseismic coupling, segmentation and mechanical behavior of the central Chile subduction zone. J. Geophys. Res. 117. B03406, http://dx.doi.org/10.1029/2011JB008736.

Moreno, M., et al., 2012. Toward understanding tectonic control on the Mw 8.8 2010 Maule Chile earthquake. Earth Planet. Sci. Lett. 321–322, 152–165, http://dx.doi.org/10.1016/j.epsl.2012.01.006.

Moscoso, E., Grevemeyer, I., Contreras-Reyes, E., Flueh, E.R., Dzierma, Y., Rabbel, W., Thorwart, M., 2011. Revealing the deep structure and rupture plane of the 2010 Maule, Chile earthquake (Mw = 8.8) using wide angle seismic data. Earth Planet. Sci. Lett. 307 (1–2), 147–155.

Nippress, S.E.J., Rietbrock, A., 2007. Seismogenic zone high permeability in the Central Andes inferred from relocations of micro-earthquakes. Earth Planet. Sci. Lett. 263, 235–245.

Okada, Y., 1985. Surface deformation due to shear and tensile faults in a half-space. Bull. Seismol. Soc. Am. 75, 1135–1154.

Pardo, M., Comte, D., Monfret, T., Boroschek, R., Astroza, M., 2002. The October 15, 1997 Punitaqui earthquake (Mw = 7.1): A destructive event within the subducting Nazca plate in central Chile. Tectonophysics 345, 199–210.

Rietbrock, A., Ryder, I., Hayes, G., Haberland, C., Roecker, S., Lyon-Caen, H., 2012. Aftershock seismicity of the 2010 Maule Mw = 8.8, Chile, earthquake: Correlation between co-seismic slip models and aftershock distribution? Geophys. Res. Lett. 39. L08310.

Rosen, P.A., Henley, S., Peltzer, G., Simons, M., 2004. Updated repeat orbit interferometry package released. Eos 85, 47.

Ruegg, J.C., Rudloff, A., Vigny, C., Madariaga, R., de Chabalier, J.B., Campos, J., Kausel, E., Barrientos, S., Dimitrov, D., 2009. Interseismic strain accumulation measured by GPS in the seismic gap between Constitución and Concepción in Chile. Phys. Earth Planet. Inter. 175 (1–2), 78–85.

Ruiz, S., Madariaga, R., 2011. Determination of the friction law parameters of the Mw 6.7 Michilla earthquake in northern Chile by dynamic inversion. Geophys. Res. Lett. 38. L09317, http://dx.doi.org/10.1029/2011GL047147.

Ruiz, S., Kausel, E., Campos, J., Saragoni, G.R., Madariaga, R., 2011. Identification of high frequency pulses from earthquake asperities along Chilean subduction zone using strong motion. Pure Appl. Geophys. 168 (1–2), 125–139.

Ruiz, S., Madariaga, R., Astroza, M., Saragoni, G.R., Lancieri, M., Vigny, C., Campos, J., 2012. Short period rupture process of the 2010 Mw 8.8 Maule earthquake in Chile. Earthq. Spectra 28 (S1), S1–S18.

Ryder, I., Rietbrock, A., Kelson, K., Bürgmann, R., Floyd, M., Socquet, A., Vigny, C., Carrizo, D., 2012. Large extensional aftershocks in the continental forearc triggered by the 2010 Maule earthquake, Chile. Geophys. J. Int. 188 (3), 879–890, http://dx.doi.org/10.1111/j.1365-246X.2011.05321.x.

Satriano, C., Kiraly, E., Bernard, P., Vilotte, J.-P., 2012. The 2012 Mw 8.6 Sumatra earthquake: Evidence of westward sequential seismic ruptures associated to the reactivation of a N–S ocean fabric. Geophys. Res. Lett. 39 (15). L15302, http://dx.doi.org/10.1029/2012GL052387.

Tassara, A., Götze, H.-J., Schmidt, S., Hackney, R., 2006. Three-dimensional density model of the Nazca plate and the Andean continental margin. J. Geophys. Res. 111. B09404, http://dx.doi.org/10.1029/2005JB003976.

Tong, X., et al., 2010. The 2010 Maule, Chile earthquake: Downdip rupture limit revealed by space geodesy. Geophys. Res. Lett. 37. L24311, http://dx.doi.org/10.1029/2010GL045805.

Vallée, M., Bouchon, M., 2004. Imaging coseismic rupture in far field by slip patches. Geophys. J. Int. 156 (3), 615–630.

Vigny, C., Socquet, A., Peyrat, S., Ruegg, J.-C., Métois, M., Madariaga, R., Morvan, S., Lancieri, M., Lacassin, R., Campos, J., Carrizo, D., Bejar-Pizarro, M., Barrientos, S., Armijo, R., Aranda, C., Valderas, M.-C., Ortega, I., Bondoux, F., Baize, S., Lyon-Caen, H., Pavez, A., Vilotte, J.P., Bevis, M., Brooks, B., Smalley, R., Parra, H., Baez, J.-C., Blanco, M., Cimbaro, S., Kendrick, E., 2011. The 2010 Mw 8.8 Maule megathrust earthquake of Central Chile, monitored by GPS. Science 331, 1417–1421.

Yagi, Y., Nakao, A., Kasahara, A., 2012. Smooth and rapid slip near the Japan Trench during the 2011 Tohoku-oki earthquake revealed by a hybrid back-projection method. Earth Planet. Sci. Lett. 355–356, 94–101, http://dx.doi.org/10.1016/j.epsl.2012.08.018.

Yao, H., Shearer, P., Gerstoft, P., 2012. Subevent location and rupture imaging using iterative back-projection for the 2011 Tohoku Mw 9.0 earthquake. Geophys. J. Int. 190, 1152–1168, http://dx.doi.org/10.1111/j.1365-246X.2012.05541.x.

Yao, H., Shearer, P., Gerstoft, P., 2013. Compressive sensing of frequency-dependent seismic radiation from subduction zone megathrust ruptures. Proc. Natl. Acad. Sci. USA 110 (12), 4512–4517, http://dx.doi.org/10.1073/pnas.1212790110.